Volume 24
Number 3
7 February 2022
Pages 963-1376

Green Chemistry

Cutting-edge research for a greener sustainable future

rsc.li/greenchem

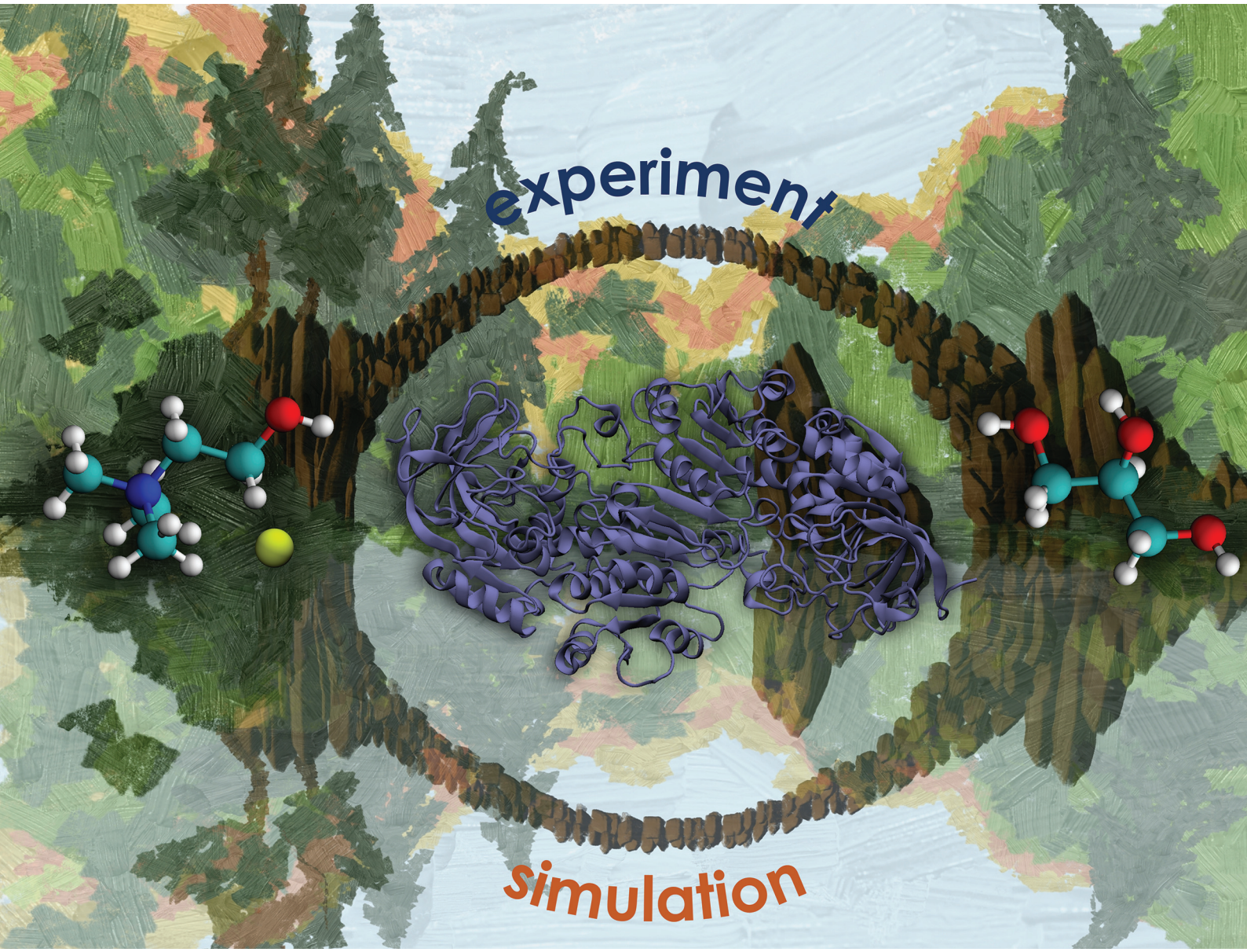

ISSN 1463-9262

ROYAL SOCIETY OF CHEMISTRY

PAPER

Sven Jakobtorweihen, Selin Kara *et al.*
Impact of deep eutectic solvents (DESs) and individual DES components on alcohol dehydrogenase catalysis: connecting experimental data and molecular dynamics simulations

Green Chemistry

PAPER

View Article Online
View Journal | View Issue

Cite this: *Green Chem.*, 2022, **24**, 1120

Impact of deep eutectic solvents (DESs) and individual DES components on alcohol dehydrogenase catalysis: connecting experimental data and molecular dynamics simulations†

Jan Philipp Bittner, ‡[a] Ningning Zhang,‡[b] Lei Huang,[b] Pablo Domínguez de María,[c] Sven Jakobtorweihen *[a,d] and Selin Kara *[b]

For a knowledge-based design of enzyme catalysis in deep eutectic solvents (DESs), the influence of the DES properties (*e.g.*, water activity and viscosity) and the impact of DESs and their individual components must be assessed. This paper investigates three different DESs: choline chloride–glycerol (ChCl–Gly), choline chloride–ethylene glycol (ChCl–EG), and ethyl ammonium chloride–glycerol (EACl–Gly). The specific activity and half-life time of horse liver alcohol dehydrogenase (HLADH) were experimentally determined in these DESs with water contents ranging from 0%–100%. HLADH showed limited activity in neat DESs, which was enhanced by adding water. Experiments with individual DES components of ChCl–Gly were carried out to clarify their individual influence. Glycerol acts as a strong stabilizer for the enzyme, whereas choline chloride's results are deleterious. To understand the experimental findings, molecular dynamics (MD) simulations were carried out to quantify the solvation layer and calculate the spatial distribution of the solvent molecules around HLADH. The experimental and the *in silico* approach suggests that designing novel DESs with higher glycerol loadings would result in improved media for biocatalysis. This is demonstrated by performing the reduction of cinnamaldehyde to cinnamyl alcohol—a relevant compound for the food industry and cosmetics—in ChCl–Gly (1 : 9 molar ratio), with 20 vol% water to decrease the viscosity. HLADH is highly active and stable under these new conditions, giving promising productivity (15.3 g L^{-1} d^{-1}). This paper demonstrates that DESs can be designed to be both substrate-solubilizers and enzyme-compatible, opening new research lines for green chemistry and biocatalysis.

Received 31st October 2021,
Accepted 6th December 2021

DOI: 10.1039/d1gc04059f

rsc.li/greenchem

Introduction

The application of nature's catalysts 'enzymes' for the synthesis of chemicals is a key emerging field to meet the current and future needs for sustainable manufacturing of chemicals.[1] Solvents play a key role in catalysis, with relevant impact on the development of efficient and green(er) syntheses. To date, the number of environmentally acceptable solvents has been limited, and alternatives are of high interest.[2,3] In recent years, deep eutectic solvents (DESs) have gained great attention as promising solvents for biocatalysis.[4–6] In fact, DESs have even been coined as 'the solvents of the 21st century'.[7] In a nutshell, DESs' assets are based on their often biogenic origin and their properties such as melting points below room temperature, low volatility, high thermal stability, tunability analogous to ionic liquids (ILs), biodegradability, large availability at acceptable costs, and straightforward preparation.[8] In particular, the high degree of freedom in designing DESs from a variety of (biogenic) substances enables the creation of a 'sustainable' solvent platform.[9]

DESs, as first described by Abbott *et al.*,[10] are binary eutectic mixtures usually formed by combining a quaternary ammonium salt (*e.g.*, choline chloride (ChCl)) acting as a hydrogen bond acceptor (HBA) with a hydrogen bond donor (HBD, *e.g.*, urea and glycerol). Importantly, the presence of hydrogen bond donor–acceptor partners in the solution may

[a]*Institute of Thermal Separation Processes, Hamburg University of Technology, Eißendorfer Straße 38, 21073 Hamburg, Germany. E-mail: jakobtorweihen@tuhh.de*
[b]*Biocatalysis and Bioprocessing Group, Department of Biological and Chemical Engineering, Aarhus University, Gustav Wieds Vej 10, 8000 Aarhus, Denmark. E-mail: selin.kara@bce.au.dk*
[c]*Sustainable Momentum, SL., Av. Ansite 3, 4-6, 35011 Las Palmas de Gran Canaria, Canary Islands, Spain*
[d]*Department for Chemical Reaction Engineering, Hamburg University of Technology, Eißendorfer Straße 38, 21073 Hamburg, Germany*
†Electronic supplementary information (ESI) available. See DOI: 10.1039/d1gc04059f
‡Both authors contributed equally to this work and are ordered alphabetically.

not be enough to characterize a 'deep' eutectic. In fact, the melting point of the deep eutectic has to be lower than that of the eutectic of an ideal solution, indicating strong attractive interactions between the DES constituents.[11] This non-ideal behavior is a key property of DESs as reaction media for biocatalysis as it lowers the reactivity of the DES components and stabilizes the enzyme structure. For instance, Gorke *et al.* documented the first DES application in lipase-catalysis and revealed that the individual components within the DESs are 20 to >600-fold less reactive as substrates than expected based on their concentrations.[12] This lowered reactivity was found to be 2–4 kcal mol^{-1}, analogous to the energy of hydrogen bond formation between the DES constituents. Likewise, in a molecular dynamics (MD) study of *Candida antarctica* lipase B (CALB), Monhemi *et al.* showed that the structure of CALB remains stable in urea-containing DES (choline chloride–urea, a molar ratio of 1 : 2).[13] The formation of complexes between choline, chloride, and urea on the surface of CALB prevented the diffusion of urea into the enzyme structure and therefore enzyme denaturation.

Over the last decade, many biotransformations have been established involving DESs as solvents, co-solvents, additives, or even substrates in a wide variety of reaction types and enzymes.[14,15] As robust biocatalysts, lipase-catalyzed reactions in DESs have been extensively explored, *e.g.*, several (*trans*-) esterifications catalyzed by immobilized CALB in ChCl-based DES–water mixtures.[16–18] Moreover, Durand *et al.* and Kim *et al.* investigated the effects of different DES components on free lipases, reflecting the significance of understanding the interactions between DESs and enzymes.[19,20] Inspired by these pioneering studies, the use of DESs in redox biocatalysis has seen a rapid rise.[21] For example, Domínguez de María *et al.* reported the use of Baker's yeast in DES–water mixtures for the selective reduction of ethyl acetoacetate, showing complete stereo inversion depending on the DES proportion (related to buffer).[22] In addition, the use of whole cells overexpressing alcohol dehydrogenases (ADHs) in DES-aqueous media was analyzed revealing the maintenance of enzyme activity at high DES contents.[23] Very recently, Fraaije and coworkers disclosed the beneficial effects of sugar-based DESs as co-solvents on 5-hydroxymethylfurfural oxidase.[24] In addition, to optimize the biocatalytic processes in DESs, the physicochemical parameters like viscosity, water activity,[25] and oxygen transfer rates (OTRs)[26] have been explored experimentally and computationally. Despite these advances, further investigations are needed to understand the structural changes of enzymes in DESs and their interactions at the molecular level. Ultimately, the knowledge would enable the proper selection of a tailored solvent for biotransformation.

Viscosity is an important physicochemical property for solvents, as it affects mass transfer in catalytic transformations. Most DESs exhibit relatively high viscosity (>100 mPa s at room temperature, compared to water, 0.89 mPa s).[27,28] To overcome this, water can be added to DESs as a co-solvent to lower the viscosity.[29–31] This enables the set-up of continuous processes using DES–water mixtures with relatively low viscosities, leading to potential synergies for green chemistry.[32,33] The addition of up to 20 vol% water leads to a remarkable decrease of viscosity without disrupting the inherent properties of many ChCl-based DESs[29,34,35] and it may even have a structure stabilizing effect.[36]

Another property often linked to the activity of enzymes in non-conventional reaction media is the water activity (a_W) in the solvent mixture.[18] The water activity is a corrected concentration ($a_W = x_W \times \gamma_W$) that includes the interaction between water and the solvent. The activity coefficient (γ_W) describes therefore the deviation from ideality. For a model system containing an enzyme, water, and a non-aqueous solvent (Scheme 1), the water molecules in the mixture will be distributed between the protein surface and the bulk phase. The above described two regions are in constant exchange, meaning that water molecules will constantly "adsorb" onto and "desorb" from the enzyme surface. The equilibrium of this constant exchange from the surface of the enzyme—the resulting enzyme hydration—will be significantly determined by the interaction of water with the solvent, and hence by a_W. While it is difficult to measure the hydration of an enzyme experimentally, its determination from MD simulations is straightforward. Using this concept, Wedberg *et al.*[37] could relate the hydration of CALB in organic solvents to the a_W values of the solvents. In general, this methodology allows the estimation of the enzyme-bound water that is necessary to maintain the enzymatic activity in non-conventional media, and hence to relate the enzyme hydration to a_W in the bulk phase and to serve for future solvent screening.

In general, MD simulations lead to detailed atomistic insights into the enzyme behavior in a specific reaction medium and can unravel structural changes and the interactions between the enzyme and solvents, which can then be correlated experimentally. MD simulations have mainly been utilized to study lipases in organic solvents and DESs,[13,37–39] but recently other enzymes have also gained attention for studying their behavior in different solvents with molecular

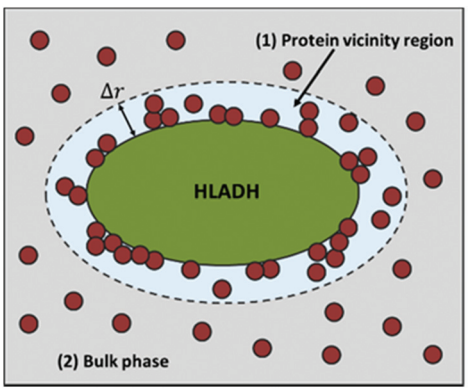

Scheme 1 Illustration of the distribution of water around an enzyme in a non-aqueous solvent. The space around the enzyme can be distributed into two different regions: (1) a *protein vicinity region*, where the interaction of water with the protein (here shown horse-liver alcohol dehydrogenase, HLADH) dominates, and (2) a *bulk phase*, where the interaction of water with the solvent mixture is dominant.

methods.[40,41] Importantly, the underlying models of MD simulations are interaction models (the so-called force field). Existing biomolecular force fields have recently been tuned towards DESs[42–45] and have already been validated for their performance in enzyme simulations and as such the applicability of MD for enzymes in DESs has been proven.[46]

The enzymatic activity of ADHs could be maintained in DES–water mixtures (>10 vol% water) and outperformed pure DESs, illustrating the benefits of adding water.[40,47] The effects of individual DES components on enzyme catalysis, together with the determination of the optimal water concentration, have to be addressed for a practical application of DESs. Previously, we reported an analysis of the bioreduction catalyzed by horse-liver alcohol dehydrogenase (HLADH) in a choline chloride and glycerol DES (ChCl–Gly, molar ratio 1 : 2) using up to 20 vol% of water.[40] The activity and stability of the model ADH underlined a detrimental effect of ChCl–Gly (1 : 2)–water mixtures at low water concentrations. MD simulations attributed this to the reduced hydration and conformational flexibility of HLADH in DES–water mixtures. Two key properties of DES–water mixtures that influence the enzymatic performance were pinpointed: (1) reduced water activity (a_W) and (2) high viscosity (η). It remained unclear which of these two properties had the largest impact on HLADH's performance.

This paper aims at shedding light on the effect of DES–water mixtures on HLADH through different research objectives: (i) to determine the optimal water amount by gradually adding water to the ChCl–Gly (1 : 2)–water mixture up to 1 (mol mol^{-1}); (ii) to gain a deeper understanding of the effect of the individual DES components, by changing the HBD and HBA (Scheme 2). To this end, apart from ChCl–Gly (1 : 2), two other eutectic mixtures, namely choline chloride–ethylene glycol (ChCl–EG, 1 : 2) and ethyl ammonium chloride–glycerol (EACl–Gly, 1 : 1.5), are introduced; (iii) to evaluate different molar ratios of ChCl–Gly far from the eutectic point at 1 : 2. Experimental findings and MD simulations are brought together to obtain a comprehensive picture of the effects of these solvents on ADH's catalytic performance; and (iv) to generate knowledge to enable the design of a suitable DES for ADH-catalyzed reductions. The designed DES will possess adequate viscosity and enzyme-compatibility for sustainable processes in non-conventional media. Creating new environment-friendly DESs with higher compatibility for enzymes would create a new path to align green solvents and (bio)catalysis.

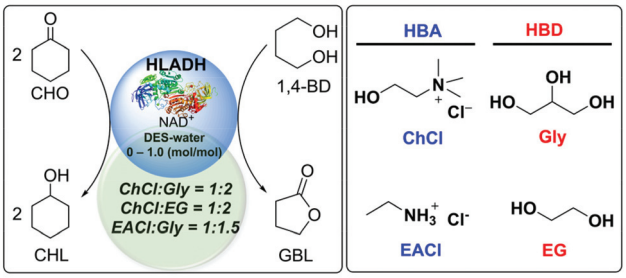

Scheme 2 Reduction of cyclohexanone (CHO) catalyzed by HLADH to cyclohexanol (CHL) promoted by 1,4-butanediol (1,4-BD) in DES–water mixtures as reaction media. HBA: hydrogen bond acceptor, HBD: hydrogen bond donor, ChCl: choline chloride, EACl: ethyl ammonium chloride, Gly: glycerol, EG: ethylene glycol.

Experimental

Materials

Chemicals, cultivation media components, and reagents were purchased from Sigma-Aldrich (St Louis, USA), Carl Roth (Karlsruhe, Germany), and VWR (Radnor, US) and used as received. The Ni-NTA affinity resin was ordered from Expedeon (Cambridgeshire, UK) and a BCA protein quantification kit (Pierce™) was purchased from Thermo Scientific (Rockford, USA). The recombinant pET-28b plasmid containing the HLADH gene was from Assoc. Prof. Dr Diederik Johannes Opperman (University of Free State, South Africa).

Preparation of DESs and DES–water mixtures

Commercial names have been given to many choline chloride based DESs according to their HBD, glyceline (glycerol), ethaline (ethylene glycol) or reline (urea). To avoid the misleading impression of DESs being a new substance rather than a binary mixture, this paper follows the widely used convention of naming the DESs by their ingredients followed by their molar ratio (*e.g.*, ChCl–Gly (1 : 2) and ChCl–EG (1 : 2)). Fig. S7† shows the phase diagram of eutectics at different glycerol mole fractions for ChCl–Gly.

For ChCl–Gly (1 : 2), choline chloride and glycerol were directly weighed in a flask in a molar ratio of 1 : 2 [0.25 mol (34.9 g): 0.5 mol (46.0 g)]. The mixture was heated and stirred at 80 °C and 300 rpm until a colorless liquid was formed (*ca.* 1 hour). The same procedure was used to prepare ChCl–Gly (1 : 9).

For ChCl–EG (1 : 2), choline chloride and ethylene glycol (EG) were directly weighed in a flask in a molar ratio of 1 : 2 [0.25 mol (34.9 g): 0.5 mol (31.0 g)]. The mixture was heated and stirred at 80 °C and 300 rpm until a colorless liquid was formed (*ca.* 2 hours).

For EACl–Gly (1 : 1.5), ethyl ammonium chloride (EACl) and glycerol were directly weighed in a flask in a molar ratio of 1 : 1.5 [0.30 mol (24.5 g): 0.45 mol (41.5 g)]. The mixture was heated and stirred at 95 °C and 300 rpm until a colorless liquid was formed (*ca.* 2 hours).

DESs' properties are listed in Table S1† and the details of DES–water mixture preparation are provided in the ESI.† The conversion between volume fractions (vol%) and mole fractions of water (x_W, mol mol^{-1}) used in this work can be determined based on eqn (S1)† and found in Table S2 (ESI†).

Preparation of lyophilized purified HLADH

Fermentation and expression. The heterologous expression of HLADH was performed in *E. coli* BL21 (DE3) containing the plasmid pET28b(+)-HLADH-His. The pre-culture was grown in

a 20 mL LB medium containing 50 μg mL^{-1} kanamycin at 37 °C and 120 rpm overnight (~16 hours). Afterwards, 10 mL (2.5 vol%) of the pre-culture was used to inoculate a 400 mL LB medium containing 50 μg mL^{-1} kanamycin, which was incubated at 37 °C and 120 rpm. When the OD_{600} reached 0.6–0.8, IPTG was added to a final concentration of 0.5 mM and the incubation was continued at 24 °C for 24 hours. The cells were harvested by centrifugation at 8000 rpm at 4 °C for 10 min. The obtained cell pellets were re-suspended in a lysis buffer (50 mM NaH_2PO_4, 300 mM NaCl, 10 mM imidazole, pH 8.0) in a ratio of 40 mL lysis buffer to 20 g wet cells. The re-suspended cells were disrupted by ultrasonication (Sartorius Labsonic M with MS 73 probe) on ice at 60% amplitude (2 s. on, 8 s. off, 2 min × 5 cycles). The water-soluble protein was separated from the cell debris by centrifugation at 13 000 rpm for 45 min at 4 °C.

Enzyme purification

The obtained clear cell-free extract (CFE) was filtered with a 0.45 μm membrane and applied to the Ni-NTA column, which was previously equilibrated with 5 column volumes (CV) of wash buffer (50 mM NaH_2PO_4, 300 mM NaCl, 20 mM imidazole, pH 8.0). The column was then washed with 10 CV of wash buffer followed by 3 CV of elution buffer (50 mM NaH_2PO_4, 300 mM NaCl, 250 mM imidazole, pH 8.0) to elute the bound target enzyme. All fractions were collected for subsequent SDS-PAGE analysis. For the removal of imidazole and storage, the column was washed with the following buffers in order: (1) 5 CV of wash buffer, (2) 3 CV of MES buffer, (3) 5 CV of deionized water, and (4) 3 CV of 30 vol% ethanol. All fractions containing purified HLADH based on the SDS-PAGE analysis (Fig. S1, ESI†) were collected and dialyzed (Dialysis tubing with MWCO 14 kDa) against a desalting buffer (10 mM Tris–HCl, pH 7.5) at 4 °C. The obtained purified HLADH was fast-frozen with liquid nitrogen and subsequently freeze-dried to obtain the lyophilized powder ready to use.

Determination of the thermodynamic water activity (a_W)

5 mL of freshly prepared DESs and DES–water mixtures were incubated at 25 °C in 30 mL sealed glass bottles for 3 days. The thermodynamic water activity (a_W) of the DES–water mixtures was determined at room temperature (25 °C) using an HMT337 Humidity Sensor (Vaisala, Finland). Here, the a_W values were measured based on the ratio of the water vapor pressure (p) in the DES–water mixtures to the vapor pressure of pure water (p_0) ($a_W = p/p_0$).

Determination of the dynamic viscosity (η)

The dynamic viscosity (η) of the DES–water mixtures was measured with a 2 mL sample using a Brookfield Digital Rheometer (Model DV-III Ultra, Brookfield Engineering Laboratories Inc., MA, USA) equipped with a spindle CPE41 at different shear rates between 0.2 s^{-1} and 500 s^{-1} at room temperature (25 °C).

Determination of the specific activity of HLADH

10.4 μL of cyclohexanone and 4.4 μL of 1,4-butanediol were dissolved in the corresponding reaction media in 1.5 mL GC vials and kept at room temperature overnight for equilibration (Tables S3 and S4, ESI†). The stock of NAD^+ (20 mM) and freshly lyophilized purified HLADH (20 mg mL^{-1}) were prepared in Tris–HCl (50 mM, pH 7.5) and incubated at 25 °C for 30 min. The reactions were started by the addition of 50 μL of HLADH and NAD^+ stock solutions into the above-equilibrated reaction media. All reaction components (cyclohexanone, 1,4-butanediol, DESs, water (in the form of Tris–HCl buffer), NAD^+ and HLADH) of each reaction system were applied in 1.5 mL GC vials based on the corresponding water contents (DESs with various water contents of 0–100 vol%, ChCl with 40 vol% water, glycerol with 40 vol% water) and incubated at 25 °C and 1200 rpm. Each final system had a total volume of 1.0 mL and contained 100 mM cyclohexanone, 50 mM 1,4-butanediol, 1 mg mL^{-1} HLADH, 1 mM NAD^+ and various water contents. Each reaction was performed in duplicate. Samples were taken at definite time intervals (2–6 min) when product yields were less than 10% and analyzed with GC (Table S5†). More specific details can be found in section 4 of the ESI.† Besides, the experimental details for the reduction of cinnamaldehyde are in section 5 of the ESI.†

Determination of the half-life time of HLADH

The half-life times of HLADH were determined by incubating 500 μL of 1.0 mg mL^{-1} purified HLADH solution at 60 °C in three DESs with water contents of 0–100 vol%, ChCl with 40 vol% water, and glycerol with 40 vol% water. The corresponding incubation media was placed in 1.5 mL microcentrifuge tubes and kept at room temperature overnight for equilibration (Tables S7 and S8, ESI†). 25 μL of HLADH stock solution (20 mg mL^{-1}) was mixed with the above-equilibrated solution and was incubated at 60 °C. Aliquot samples (≥5) were taken at specific time intervals and diluted with Tris–HCl (50 mM, pH 7.5). The residual activities were measured using 1 mL reaction system (Tris–HCl [50 mM, pH 7.5], 50 mM cyclohexanone, 0.2 mg mL^{-1} heated HLADH samples, and 0.1 mM NADH) with a photometer for 1 min at 25 °C. The half-life times were determined from the plots of the natural logs of residual activities *versus* the incubation time and calculated based on eqn (S2) (ESI†). Each reaction was performed in duplicates. More details can be found in section 7 of the ESI.†

Computational methods

Force fields

Previously, we presented a comprehensive evaluation of existing biomolecular force fields for DESs and identified a modification of the General Amber Force Field (GAFF-DES) developed by Perkins *et al.*[42] as a suitable model for the simulation of HLADH in ChCl–Gly (1 : 2)– and ChCl–EG (1 : 2)–water mixtures.[46] In particular, the viscosity at low water contents was better described by GAFF-DES compared to the other tested force fields. Thus, to represent ChCl in the MD simulations of ChCl–Gly (1 : 2) and ChCl–EG (1 : 2), this modification of GAFF[48] for DESs was used. To represent the interaction of the

protein in these mixtures, the Amber03* force field[49] has been used. Electrostatic interactions have been implemented using a cut-off radius of 0.9 nm and the Lennard–Jones (LJ) potential has been shifted to zero at 0.9 nm.

To simulate HLADH in the ChCl–water mixtures, the topologies and parameters were taken from the CHARMM General Force Field (CGenFF) version 4.1.[50,51] To represent the protein in the simulations of ChCl–water mixtures, the CHARMM36m force field[52] was used. In a previous publication,[46] we showed that the behavior of HLADH is similarly described by different force fields as long as the interaction model gave a satisfying representation of the DES interactions. In the case of CGenFF, the cut-off radius for electrostatics and LJ interactions was 1.2 nm, whereby the forces were smoothly switched between 1.0 and 1.2 nm.

The GAFF-DES force field does not include parameters for EACl–Gly. Therefore, the topologies and force field parameters for representing EACl–Gly (1 : 1.5) in the MD simulations have been taken from the Optimized Potential for Liquid Simulations–All Atom (OPLS-AA) force field.[53,54] To improve the dynamic behavior of glycerol in the simulations, the CCCO, OCCO, and HCOH dihedrals of glycerol have been adjusted.[46,55,56] To represent the protein in the simulations of EACl–Gly (1 : 1.5)–water mixtures, the OPLS-AA/M force field[57,58] was used. In the case of the OPLS-AA, the LJ and electrostatic values were calculated with a cut-off radius of 1.1 nm, whereas the forces were smoothly switched between 0.9 and 1.1 nm.

Water is modeled with TIP3P[59] in all simulations with the exception of the simulations using CGenFF, where the CHARMM-TIP3P variant[60,61] was used.

Long-ranging electrostatics are calculated using the smooth particle-mesh Ewald[62] (PME) method with a PME order of 4 in all simulations.

Simulation of protein systems

All MD simulations were performed with the software GROMACS version 2019.4.[63–65] The simulation procedure for the systems including HLADH was based on prior publications.[40,46] First, cubic boxes with a box length of 13.6 nm including the enzyme structure (HLADH, PDB entry 6O91)[66] and solvent mixtures were constructed using the packmol software.[67] Energy minimization using the steepest decent algorithm is performed for 5000 steps while constraining all heavy protein atoms. The bonds to hydrogen atoms were restrained using SETTLE[68] for water and LINCS[69] for all other molecules. The temperature of the system was adjusted to 298.15 K by the velocity rescale thermostat[70] with a time constant of τ_T = 1ps in a 2 ns NVT simulation using the leap-frog integrator[71] and a time step of 1 fs, whereby in the next steps it was increased to 2 fs. The temperature was then increased to 500 K during 1 ns and kept at 500 K for 20 ns to allow better equilibration of the highly viscous DES–water mixtures. After cooling the system back to 298.15 K, the protein structure was stepwise released in two consecutive NVT simulations for 0.5 ns each by first constraining the backbone and then the C_α-atoms of HLADH. This release of the protein structure allows for a proper equilibration of the surrounding solvent without artificially distorting the protein structure. In a 2 ns NPT equilibration, the pressure is adjusted to 1 bar using the Berendsen barostat.[72] The equilibration is followed by a sampling run for 100 ns in the NPT ensemble, whereby the last 40 ns are used for computing the structural properties of HLADH as well as its interactions with the solvents. Here the pressure was controlled by the Parrinello–Rahman barostat[73] with a time constant of τ_P = 5 ps and an isothermal compressibility of $\kappa_T = 5 \times 10^{-5}$ bar^{-1}. To enhance statistical significance, duplicate simulations starting from independent initial positions and initial velocities were performed for each system.

Analysis of the MD simulations

The molecular dynamics simulations were used to calculate the root mean square fluctuations (RMSF), intra-protein hydrogen bonds (r_{HB} = 0.35 nm, ϕ_{HB} = 30°) and the hydration and solvation layers of the DES-components. Water and chloride were considered to be in the hydration/solvation layer when the oxygen atom or chloride ion, respectively, was within 3.5 Å of any non-hydrogen protein atom. An analogous definition was applied for the DES molecules with the central carbon of choline being within 6 Å, the central carbon of EAC ion within 4 Å, the central carbon of glycerol within 5 Å and a carbon of ethylene glycol within 4 Å of any non-hydrogen protein atom.

To get uncorrelated samples from the MD simulations, the block averaging technique[74] was used for the estimation of time-dependent errors. Unless stated otherwise, the error bars indicate thereby a 95% confidence interval of block averages over the last 40 ns of the trajectory with a block size of 5 ns.

To visualize the spatial distribution of the solvent molecules around HLADH, density maps of the solvent molecules with a maximum distance of 5 Å from the protein surface were calculated using the GROmaρs[75] software for the last 40 ns of the trajectory and a spacing of 0.05 nm.

Results and discussion

For the study, three DESs with various water contents were assessed (Scheme 2). HLADH's catalytic performance in these mixtures is experimentally determined followed up by a detailed investigation of the protein behavior and interaction with the solvents by molecular methods.

Experimental analysis

In the first set of experiments, an increasing amount of water was added and the half-life time and enzymatic activity of HLADH were determined (Fig. 1). The half-life time values were dependent on the water content. Interestingly, a high half-life time peak was observed for ChCl–Gly (1 : 2) at a water mole fraction of 0.72 mol mol^{-1} (equivalent to 40 vol%), which decreased at higher water contents (Fig. 1a). Remarkably, the positive effect at x_W = 0.72 mol mol^{-1} on the stability of HLADH was even higher than the half-life time observed in the

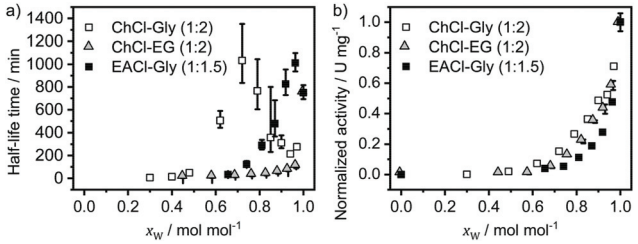

Fig. 1 (a) Half-life time of HLADH in mixtures of ChCl–Gly (1 : 2) (white squares), ChCl–EG (1 : 2) (grey triangles), and EACl–Gly (1 : 1.5) (black squares) with water in dependency of the water mole fraction x_W at 60 °C. The error bars are 95% confidence intervals based on the fit of the half-life time to an exponential decrease function. (b) Specific activity (product yields ≤10%) of HLADH in the three DES–water mixtures in dependency of the water mole fraction x_W at 25 °C and normalized by the specific activity in the aqueous buffer. The error bars are calculated from duplicated experiments.

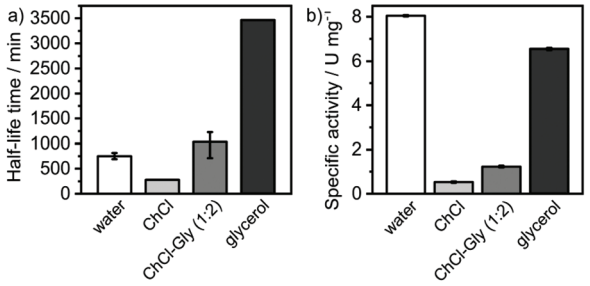

Fig. 2 (a) Half-life time of HLADH in water, ChCl–Gly (1 : 2)-, ChCl– and glycerol–water mixtures with 40 vol% water at 60 °C. (b) Specific activity (product yields ≤10%) of HLADH-catalyzed reduction in the different systems with 40 vol% water at 25 °C. The error bars are calculated from duplicated experiments.

aqueous buffer. It has been reported that at 0.72 mol mol^{-1}, the typical DES hydrogen bond network starts to get disrupted[46] and the DESs molecules are either present in small clusters or individually hydrated.[76] Strikingly, EACl–Gly (1 : 1.5) showed again a high half-life time peak, yet shifted towards larger water contents (0.96 mol mol^{-1}). Conversely, in ChCl–EG (1 : 2), a smooth increase in half-life time preceded along with the water contents and no peaks were observed. Taken together, these results suggest that the presence of glycerol in the DESs may play a role in the high stability peak observed for HLADH.

Subsequently, the specific activity of HLADH in the different DES–water mixtures was investigated by performing the HLADH-catalyzed reduction of cyclohexanone in the DES–water mixtures with the water mole fraction x_W (mol mol^{-1}) ranging from 0 to 1 (Scheme 2). An aqueous buffer solution (50 mM Tris–HCl, pH 7.5) was used for comparison. The specific activity of HLADH was calculated based on product yields per time (product yields ≤10%) and normalized by the activity in the aqueous buffer. In contrast to the half-life time of HLADH, the specific activity of HLADH increased gradually with increasing water content up to a maximum in the aqueous buffer (Fig. 1b). This illustrates the general detrimental effect of the three studied DESs on the activity of HLADH, which can be alleviated by the addition of water, consistent with our previous study.[40]

In general, DESs are binary mixtures, and thus the discrepancy between the stability and the specific activity of HLADH was studied by analyzing the individual contributions of ChCl and glycerol, whereby the volume fraction of water remained constant at 40 vol% (Fig. 2) (Table S3†). The half-life time of HLADH in ChCl with 40 vol% water was 277 min, while in glycerol with 40 vol% water it was 3466 min (Fig. 2a). This demonstrates the beneficial effect of glycerol on enzyme stability, which exceeds the stability of the aqueous buffer by a factor of 4.5 (Fig. 2a). The use of ChCl–Gly (1 : 2) suggested a more detrimental influence of ChCl than a stabilizing effect of glycerol. Analogous results for glycerol and ChCl have been reported for other enzymes (*e.g.*, glycosidases).[77] Overall, the reduced stability observed in the ChCl–Gly (1 : 2) mixtures may be mostly caused by ChCl. Besides, we also analyzed the equilibration of the highly viscous DES–water mixtures by following different preparation routes (A and B) of ChCl–Gly (1 : 2)–water mixtures. The details on the preparation of the reaction mixtures and assays for specific activity and half-life time analyses can be found in the ESI (sections 4.2 and 7.2, ESI†). The different equilibration methods resulted in the same solution conditions and catalytic outputs proving that the highly viscous DES solutions can be well equilibrated not only by heating and stirring for short time but also by simply mixing for longer times (Fig. S2 and S3, ESI†).

In addition to the half-life time, the specific activity of HLADH was assessed based on the initial rates (product yields ≤10%). Compared with ChCl–Gly (1 : 2)–water (40 vol%), the specific activity of HLADH in the ChCl–water mixture was lower, while the corresponding glycerol–water mixture resulted in a higher enzyme activity that is comparable to the aqueous buffer (Fig. 2b). This further emphasizes that the deleterious effect of ChCl–Gly (1 : 2) on HLADH is caused by ChCl.

Overall, the results suggest that pure glycerol would be the preferred media for enzymatic reactions. However, the high viscosity of glycerol, together with the need for dissolving substrates that often display unpaired solubilities hampers that approach from a practical standpoint. Importantly, our results also imply that designing a DES with increasing content of glycerol—but remaining as a DES—would provide the basis to develop a more enzyme-compatible solvent with less viscosity than pure glycerol and with better handling than glycerol–water mixtures. From a green chemistry perspective, developing tailored solvents for enzymatic processes would constitute an asset to deliver improved synthetic strategies, in which substrates with unpaired solubilities can be fully dissolved and the media turns out enzyme-compatible at the same time. To validate this, the molar ratio of glycerol in ChCl–Gly was increased from 1 : 2 to 1 : 9. In line with the DES definition discussed in the introduction, the melting point of this 1 : 9 mixture is lower than that of the eutectic of an ideal 1 : 9 solution. Expectedly, the new DESs (ChCl–Gly (1 : 9)) possessed high viscosity (554 mPa s), which could be reduced to a man-

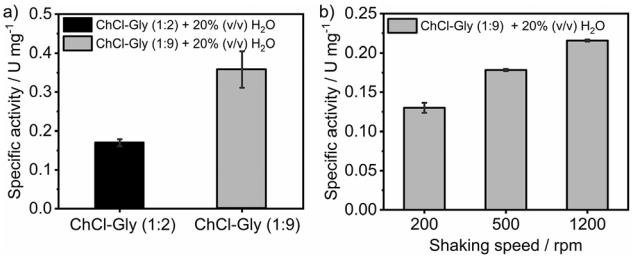

Fig. 3 (a) Comparison of specific activity (product yields ≤10%) of HLADH-catalyzed cyclohexanone reduction in ChCl–Gly (1 : 2) and ChCl–Gly (1 : 9) with 20 vol% water at 25 °C. (b) The specific activity (product yields ≤10%) of HLADH-catalyzed reduction in ChCl–Gly (1 : 9) with 20 vol% water at different shaking speeds. The error bars are calculated from duplicated experiments. The differences of activity at 1200 rpm in a and b are attributed to the use of different batches of enzyme produced.

ageable range of 50 mPa s by the addition of 20% water (Fig. S4, ESI†). Remarkably, ChCl–Gly (1 : 9) led to a two-fold higher specific activity of HLADH compared to that obtained in ChCl–Gly (1 : 2) (Fig. 3a). Thus, the generation of a DES medium with a higher content of glycerol enhances the stability and activity of HLADH. The viscosity can be ameliorated with the addition of water, and by enhancing the stirring speed, even higher enzymatic rates are achieved (Fig. 3b).

Triggered by the promising results, the new ChCl–Gly (1 : 9) was assessed for an industrially-sound reaction, namely the reduction of cinnamaldehyde to cinnamyl alcohol, which is an important compound for the synthesis of valuable chemicals (*e.g.*, cinnamyl esters and flunarizine) for the food and cosmetic industry.[78,79] The results are shown in Fig. 4, where reactions in ChCl : Gly DESs 1 : 2 and 1 : 9 with 20 vol% water are compared.

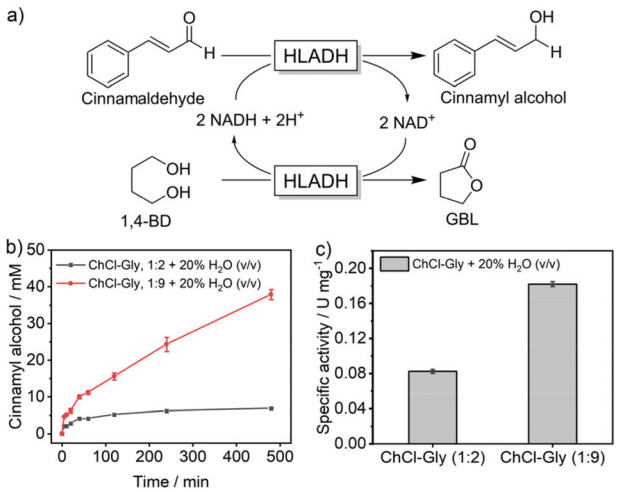

Fig. 4 (a) The HLADH-catalyzed reduction of cinnamaldehyde to cinnamyl alcohol. (b) Formation of cinnamyl alcohol over time and (c) comparison of specific activity (product yields ≤10%) of HLADH-catalyzed cinnamaldehyde reduction in ChCl–Gly (1 : 2) and ChCl–Gly (1 : 9) with 20 vol% water at 25 °C. The error bars are calculated from duplicated experiments.

In line with the conversion of cyclohexanone, the enzymatic performance in the new DESs significantly improved when compared with the reaction in the *classic* DES ChCl–Gly (1 : 2), leading to a 2.5-fold higher specific activity. In the new DESs, a 40% yield of cinnamyl alcohol was achieved in ChCl–Gly (1 : 9) with 20 vol% water in 8 h (under non-optimized conditions), while less than 7% of cinnamyl alcohol was obtained in ChCl–Gly (1 : 2). Furthermore, the new DESs seem to display a stabilizing effect for HLADH. Thus, the reaction stops after two hours in the 1 : 2 DESs, while high activity remains in the glycerol-loaded solvent. Overall, these findings prove that ChCl–Gly (1 : 9) imposed beneficial effects on HLADH and thus can be applied in various organic synthesis applications. Moreover, it suggests that new DESs with enhanced enzyme-compatibility can be designed by replacing the deleterious choline chloride with other hydrogen-bond acceptors. Combining tailored green solvents and biocatalysts can make a significant step forward for green chemistry strategies.

MD simulations

Experimental results have shown the effects of the individual DES components and addition of water on HLADH's stability and activity. However, the structural behavior of HLADH and its interactions with the DES–water mixtures are difficult to access in experiments. To fully understand the interactions of the DES components and water with the protein structure, MD simulations of HLADH at atomistic resolutions with respect to DES–water environments were performed.

One specific goal was to shed light on how the hydration layer around HLADH was built, and its dependency on the water concentration. Functioning as an indication of enzyme-bound water (Scheme 1),[80] the a_W values of the DES–water mixtures were experimentally determined. Overall, the water activity of the DES–water mixtures showed a negative deviation from the ideal mixture (Fig. S5a, ESI†), which is in line with previous reports.[40,46,81,82] This negative deviation implies strong attractive forces between the DES components and water, which resulted in reduced enzyme hydration. As shown in Fig. 5a, the hydration layers of HLADH in all DES–water mixtures display similar trends. These results also indicate the strong attractive interactions between ChCl–Gly (1 : 2), ChCl–EG (1 : 2) or EACl–Gly (1 : 1.5) molecules and water that lead to preferential solvation of water in the bulk phase rather than populating the enzyme surface. In other words, the polar DES components compete with water for polar interaction sites on HLADH's surface and therefore effectively strip water from the enzyme surface. In addition, the measured water activities of the aqueous mixtures of ChCl and glycerol reveal the strong affinity of ChCl towards interacting with water as indicated by a low water activity (a_W = 0.55) (Table S9, ESI†). The glycerol–water mixture also shows the attractive interaction between these molecules (a_W = 0.66), however, to a much lesser extent compared to ChCl. This indicates that ChCl is mainly causing the stripping of water from the enzyme surface, which can further underline the detrimental impact of ChCl on ADH catalysis (Fig. 2) Although the DES molecules can mimic the

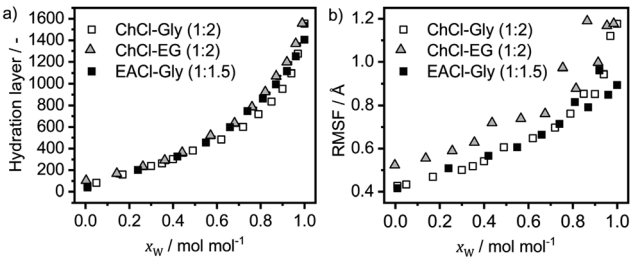

Fig. 5 (a) Time averages of the hydration layer around HLADH in mixtures of ChCl–Gly (1 : 2) (white squares), ChCl–EG (1 : 2) (grey triangles) and EACl–Gly (1 : 1.5) (black squares) with water in dependency of the water mole fraction x_W from the MD simulations. (b) Root mean square fluctuations (RMSF) of the C_α-atoms of HLADH from the MD simulations (averaged over both protein chains) in dependency of the water mole fraction x_W. The MD simulations of HLADH in the ChCl–Gly (1 : 2)- and ChCl–EG (1 : 2)–water mixtures are based on Bittner *et al.*,[46] but with more water concentrations.

interactions of water and replace water on HLADH's surface, our results emphasize that the effect of water on the structure and catalytic performance of HLADH is essential. Besides its structural effect, the presence of water at the active center of HLADH is required for the reaction itself.[83]

The increase in enzyme hydration accompanied by the increasing root mean square fluctuations (RMSF), implies enhanced enzyme flexibility (Fig. 5b) that is necessary for the formation of the enzyme–substrate complex. The effect of DES viscosity on the enzyme structure can be seen in Fig. 4b, as HLADH is more flexible in ChCl–EG (1 : 2) with lower viscosity compared to ChCl–Gly (1 : 2) or EACl–Gly (1 : 1.5). Still, the flexibility of HLADH in both DES solutions is significantly lower compared to that in the aqueous buffer. The difference between the viscosities of the three DES–water mixtures is drastically reduced for larger water concentrations (Fig. S5b, ESI†), where the enzyme activity improves.

The specific activity measurements in combination with the molecular modelling of HLADH suggest that the limited hydration of HLADH in the DES–water mixtures significantly affects the enzyme performance, while the larger viscosity of the glycerol-based DESs did not result in a lower catalytic activity compared to ChCl–EG (1 : 2).

As stated above, our experimental results showed that in contrast to the specific activity of HLADH, its stability displays significant differences in the three DESs–water mixtures, with peaks of high stability when glycerol was used as DES component (Fig. 1a). To visualize the impact of solvent molecules in direct contact with HLADH, MD simulations provided a detailed picture of solvation layers of the different DES components surrounding the enzyme. Analogous to the hydration of the enzymes, the solvation layer of the DES consists of the DES molecules in direct contact with the enzyme surface. As pointed out by Bittner *et al.*,[46] the solvation layer of the HBDs differs significantly from the trend of the HBA. While the number of choline, ethyl ammonium and chloride molecules in direct contact with the enzyme decrease nearly linearly with increasing water concentrations (Fig. 6b and c), the solvation of glycerol or ethylene glycol remains almost constant at low water concentrations (Fig. 6a). This means that the addition of water at low concentrations will trigger a replacement of the HBA ions on the surface of HLADH by water molecules, while the interaction with the HBD initially remains unchanged. As a result, the composition of the DES molecules on the enzyme surface shifts when water is added to the system. This shift of DES compositions combined with the positive impact of glycerol on HLADH's stability may explain the peak in the stability of HLADH in ChCl–Gly (1 : 2) (Fig. 1a). Up to x_W = 0.72 mol mol^{-1}, the amount of glycerol on HLADH's surface stays constant and the amount of choline and chloride decreases steadily. At x_W = 0.72 mol mol^{-1}, a large portion of ChCl was replaced by water on the surface of HLADH which in combination with a predominant presence of glycerol on its surface resulted in the experimentally observed stable enzyme.

To further underline this effect, the spatial distribution functions (SDF) of the DES components were calculated from the MD trajectories using GROmaps.[75] The resulting three-dimensional density distribution of the HBA cation (blue), chloride (yellow), HBD (green) and water (red) are exemplarily shown for selected DES–water concentrations in Fig. 7. This spatial arrangement of the DES molecules around HLADH can further highlight the positive impact of glycerol on HLADH. For ChCl–Gly (1 : 2), while choline and chloride are present on the surface at a water mol fraction of 0.01 mol mol^{-1} (HLADH not active)

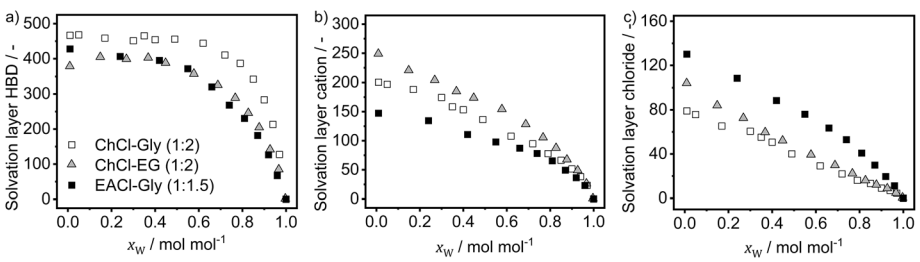

Fig. 6 Time averages of the solvation layer around HLADH in mixtures of ChCl–Gly (1 : 2) (white squares), ChCl–EG (1 : 2) (grey triangles) and EACl–Gly (1 : 1.5) (black squares) with water in dependency of the water mole fraction x_W from the MD simulations. (a) Number of molecules of HBD (glycerol or ethylene glycol) molecules in the solvation layer, (b) molecules of DES cations (choline or ethyl ammonium) in the solvation layer and (c) number of chloride ions in the solvation layer. The MD simulations of the ChCl–Gly (1 : 2)- and ChCl–EG (1 : 2)–water mixtures are based on Bittner *et al.*,[46] but with more water concentrations.

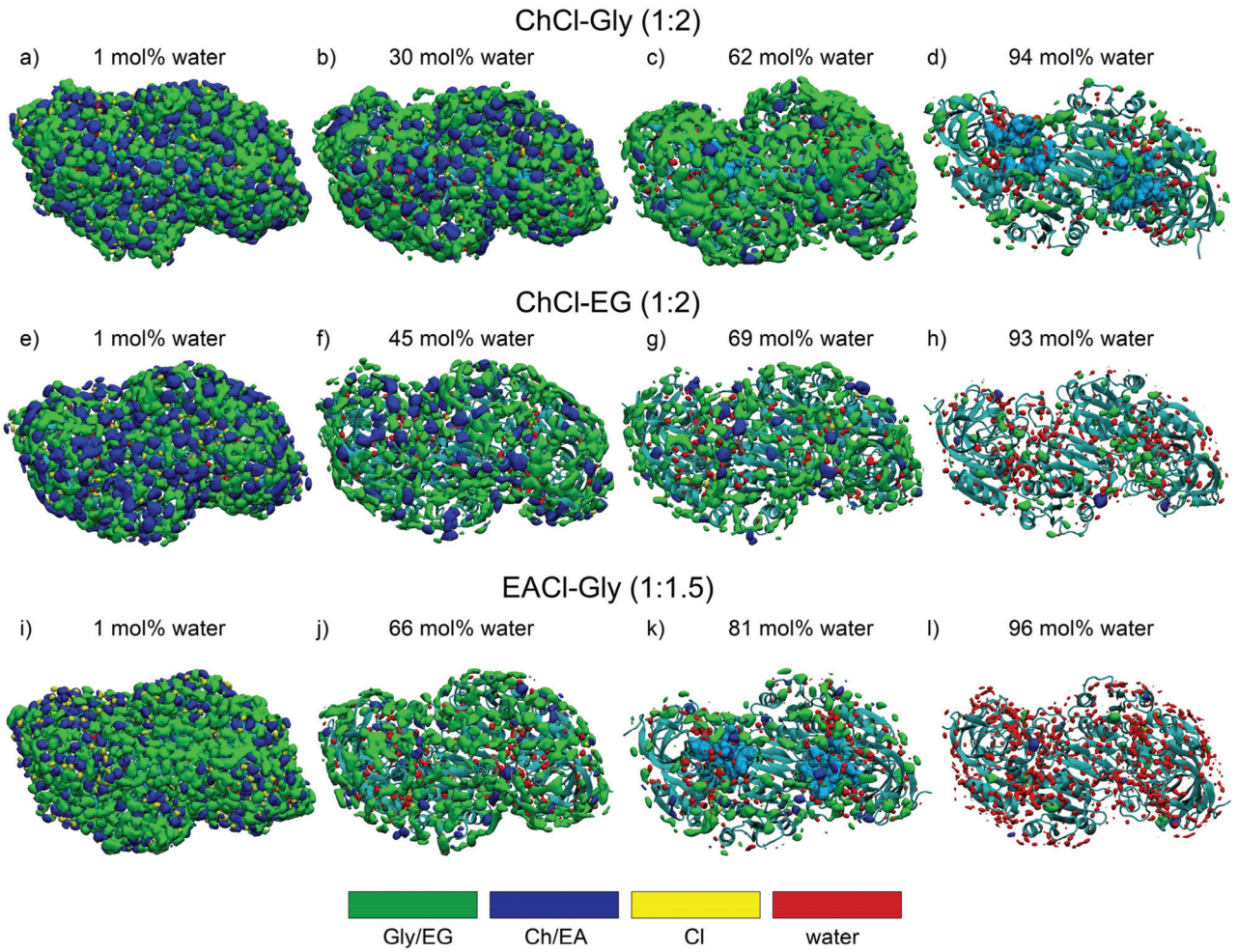

Fig. 7 Spatial distribution functions of (a–d) ChCl–Gly (1 : 2), (e–h) ChCl–EG (1 : 2) and (i–l) EACl–Gly (1 : 1.5)–water mixtures around HLADH in the MD simulations for different water concentrations created with GROmaps.[63] The shown iso-surfaces correspond to a relative spatial electron density of 0.1 e nm^{-2}. Please note that places, where no map is shown (protein visible), indicate that no specific component is located here, rather different components can be observed at these locations over time. Cyan blue: HLADH structure represented as cartoon, green: spatial density distribution of glycerol (Gly) or ethylene glycol (EG), blue: spatial density distribution of choline (Ch) or ethyl ammonium (EA), yellow: spatial density distribution of chloride (Cl) and red: spatial density distribution of water around the HLADH structure. The software VMD[84] was used for this visualization.

and of 0.3 mol mol^{-1} (HLADH activity first detected), the enzyme surface is nearly completely solvated with glycerol at x_W = 0.62 mol mol^{-1} (Fig. 7c). At larger concentrations (x_W > 0.72 mol mol^{-1}), glycerol starts to be rapidly replaced by water. This change in the solvation of HLADH is indicated by less glycerol on the protein surface (Fig. 7d) that coincides with a decrease in the enzyme stability (Fig. 1a).

The solvation layer of ethylene glycol in ChCl–EG (1 : 2)–water mixtures showed a similar trend to glycerol in ChCl–Gly (1 : 2) (Fig. 6). Instead of gradually decreasing as the solvation layers of choline and chloride, the number of HBD molecules in direct contact with HLADH remained almost constant up to an x_W of 0.5 mol mol^{-1}. This effect can additionally be seen in the SDFs (Fig. 7e–h), whereby the space occupied by ethylene glycol is reduced compared to glycerol in ChCl–Gly (1 : 2) and choline is more present on the surface of HLADH while solvated in pure DES. At higher water contents (0.93 mol mol^{-1}), the predominant interaction sites of ethylene glycol disappear (Fig. 7h). Combined with the HLADH's half-life time (Fig. 1a), this suggests that the accumulation of ethylene glycol on the enzyme surface does not have a favorable effect on enzyme stability. This means that the maximum observed half-life time in ChCl–Gly (1 : 2) can be completely attributed to the presence of glycerol and the decreasing numbers of ChCl on HLADH's surface. This aspect is experimentally corroborated by working with DES with a higher glycerol content (*e.g.*, ChCl–Gly with molar ration 1 : 9 instead of 1 : 2), where the improved activity of the enzyme is observed (Fig. 3a).

Interestingly, the second glycerol containing DES (EACl–Gly (1 : 1.5)), showed a peak of half-life time at x_W = 0.96 mol mol^{-1} (Fig. 1a). However, upon comparing the solvation layers of HLADH in EACl–Gly (1 : 2) and ChCl–Gly (1 : 2) some differences occur. The solvation of glycerol that has been previously linked to improved enzyme stability is largely reduced by

~100 molecules over the entire concentration range (Fig. 6a). This may be caused by a different HBA to HBD composition in EACl–Gly (1 : 1.5) and can explain the reduced stability of EACl–Gly (1 : 1.5) with lower water contents. Secondly, the solvation of chloride becomes more pronounced compared to the other DESs (Fig. 6c) while the amount of ethyl ammonium ions on the surface is lower compared to choline. The concentration of chloride on HLADH's surface in the MD simulations is two times higher in EACl–Gly (1 : 1.5) at an x_W of 0.66 mol mol^{-1} which coincides with its limited stability compared to the choline counterpart (ChCl–Gly (1 : 2)) with the same water concentration. The three-dimensional density distribution of the DES components and water can be seen in Fig. 7i–l. In addition, water has a stabilizing effect on HLADH as observed from the results of ChCl–EG (1 : 2). Therefore, the shifted stability peak of HLADH in EACl–Gly (1 : 1.5) with an x_W of 0.96 mol mol^{-1} may be a combination of the aforementioned effects: (1) with increasing water contents the enzyme stability tends to increase due to a beneficial effect of water, (2) the stability in the glycerol-based DESs showed a significant improvement of the stability compared to ChCl–EG (1 : 2), which (3) may be reduced by the higher solvation of chloride and therefore lower solvation of glycerol in the case of EACl–Gly (1 : 1.5).

In general, our results emphasize that the experimentally determined stability of HLADH in the different DES–water mixtures cannot be explained by a linear combination of the solvation layers from the MD simulations. This strongly suggests that not only the amount of DES molecules, in particular glycerol, but also their position on HLADH's surface plays a major role in stabilizing the enzyme structure.

Conclusions

Three DESs with different components have been used: ChCl–Gly (1 : 2), ChCl–EG (1 : 2), and EACl–Gly (1 : 1.5). Moreover, ChCl–Gly–water mixtures with different molar ratios of ChCl and glycerol ranging from 1 : 1.5 to 1 : 9 have been explored as well. Combining experimental and computational analyses, the behavior of a representative oxidoreductase, HLADH, in these DES–water mixtures and in the individual components was investigated.

HLADH needs significant amounts of water to display enzymatic activity in the three DESs. Although the activity dependency on the water content is similar for the three DESs, the enzyme stability shows huge discrepancies. By experimentally investigating the effects of the individual components of the DESs and by varying the content of the components in a DES, the different impacts of DES components were unraveled, which were explained by molecular dynamics simulations. Altogether, the different trends in the water dependency on the half-life time could be explained by the effects of the DES components and by the amount of these components in the solvation layer around the enzyme. Most importantly, glycerol is found to be beneficial for stability, especially when the solvation layer around the enzyme mainly consists of glycerol. Taking advantage of the generated knowledge, we have demonstrated that industrially-sound reactions, such as the enzymatic reduction of cinnamaldehyde to cinnamyl alcohol, can be efficiently conducted in newly designed DESs with a higher glycerol content (ChCl–Gly, 1 : 9). For green chemistry applications, the possibility of tailoring solvents to make them more enzyme-compatible represents a promising finding that may deliver novel applications in the future.

Overall, our investigations showed that only the joint forces of experimental and computational techniques may lead to a comprehensive understanding of enzyme catalysis in DESs and as such are necessary to help make these green solvents applicable for biotechnology. We believe that the enormous potential of DESs for their use in biocatalytic applications can be fully explored when an in-depth analysis of the solvent's effects is performed. It can be anticipated that not only ADHs but also other oxidoreductases (*e.g.*, oxygenases and oxidases) and other enzyme classes may benefit from the combined assessment of experimental and theoretical research.

Conflicts of interest

There are no conflicts to declare.

Acknowledgements

The authors thank the Deutsche Forschungsgemeinschaft (DFG) (grant numbers: KA 4399/3-1 and JA 2500/5-1) for the financial support. This research used computational resources provided by The North-German Supercomputing Alliance (HLRN). The authors thank Assoc. Prof. Dr Diederik Johannes Opperman (University of the Free State, South Africa) for the recombinant plasmid containing the HLADH gene. Assoc. Prof. Menglin Chen (Aarhus University, Denmark) is gratefully thanked for the use of the rheometer. Furthermore, we would also like to thank Michelle Leganger Juul Sørensen for the technical assistance.

Notes and references

1 R. Wohlgemuth, *Curr. Opin. Biotechnol.*, 2010, **21**, 713–724.
2 C. M. Alder, J. D. Hayler, R. K. Henderson, A. M. Redman, L. Shukla, L. E. Shuster and H. F. Sneddon, *Green Chem.*, 2016, **18**, 3879–3890.
3 A. D. Curzons, D. C. Constable and V. L. Cunningham, *Clean Technol. Environ. Policy*, 1999, **1**, 82–90.
4 M. Pätzold, S. Siebenhaller, S. Kara, A. Liese, C. Syldatk and D. Holtmann, *Trends Biotechnol.*, 2019, **37**, 943–959.
5 Y. Ma, P. Li, Y. Li, S. J. Willot, W. Zhang, D. Ribitsch, Y. H. Choi, R. Verpoorte, T. Zhang, F. Hollmann and Y. Wang, *ChemSusChem*, 2019, **12**, 1310–1315.
6 R. Hollenbach, K. Ochsenreither and C. Syldatk, *Int. J. Mol. Sci.*, 2020, **21**, 4342.

7 D. A. Alonso, A. Baeza, R. Chinchilla, G. Guillena, I. M. Pastor and D. J. Ramón, *Eur. J. Org. Chem.*, 2016, 612–632.
8 J. Torregrosa-Crespo, X. Marset, G. Guillena, D. J. Ramón and R. María Martínez-Espinosa, *Sci. Total Environ.*, 2020, **704**, 135382.
9 M. L. Toledo, M. M. Pereira, M. G. Freire, J. P. A. Silva, J. A. P. Coutinho and A. P. M. Tavares, *ACS Sustainable Chem. Eng.*, 2019, **7**, 11806–11814.
10 A. P. Abbott, G. Capper, D. L. Davies, R. K. Rasheed and V. Tambyrajah, *Chem. Commun.*, 2003, 70–71.
11 M. A. R. Martins, S. P. Pinho and J. A. P. Coutinho, *J. Solution Chem.*, 2018, **48**, 962–982.
12 J. T. Gorke, F. Srienc and R. J. Kazlauskas, *Chem. Commun.*, 2008, 1235–1237.
13 H. Monhemi, M. R. Housaindokht, A. A. Moosavi-Movahedi and M. R. Bozorgmehr, *Phys. Chem. Chem. Phys.*, 2014, **16**, 14882–14893.
14 P. Xu, G. W. Zheng, M. H. Zong, N. Li and W. Y. Lou, *Bioresour. Bioprocess.*, 2017, **4**, 34.
15 M. Pätzold, S. Siebenhaller, S. Kara, A. Liese, C. Syldatk and D. Holtmann, *Trends Biotechnol.*, 2019, **37**, 943–959.
16 E. Durand, J. Lecomte, B. Barea, G. Piombo, E. Dubreucq and P. Villeneuve, *Process Biochem.*, 2012, **47**, 2081–2089.
17 M. Cvjetko Bubalo, A. Jurinjak Tušek, M. VinkoviĿ, K. RadoševiĿ, V. Gaurina SrĿek and I. RadojĿiĿ RedovnikoviĿ, *J. Mol. Catal. B: Enzym.*, 2015, **122**, 188–198.
18 E. Durand, J. Lecomte, B. Barea, E. Dubreucq, R. Lortie and P. Villeneuve, *Green Chem.*, 2013, **15**, 2275–2282.
19 E. Durand, J. Lecomte, B. Barea and P. Villeneuve, *Eur. J. Lipid Sci. Technol.*, 2014, **116**, 16–23.
20 S. H. Kim, S. Park, H. Yu, J. H. Kim, H. J. Kim, Y. H. Yang, Y. H. Kim, K. J. Kim, E. Kan and S. H. Lee, *J. Mol. Catal. B: Enzym.*, 2016, **128**, 65–72.
21 V. Gotor-Fernández and C. E. Paul, *J. Biotechnol.*, 2019, **293**, 24–35.
22 Z. Maugeri and P. Domínguez de María, *ChemCatChem*, 2014, **6**, 1535–1537.
23 C. R. Müller, I. Lavandera, V. Gotor-Fernández and P. Domínguez de María, *ChemCatChem*, 2015, **7**, 2654–2659.
24 G. de Gonzalo, C. Martin and M. W. Fraaije, *Catalysts*, 2020, **10**, 447.
25 E. L. Smith, A. P. Abbott and K. S. Ryder, *Chem. Rev.*, 2014, **114**, 11060–11082.
26 N. Zhang, F. Steininger, L.-E. Meyer, K. Koren and S. Kara, *ACS Sustainable Chem. Eng.*, 2021, **9**, 8347–8353.
27 Q. Zhang, K. De Oliveira Vigier, S. Royer and F. Jerome, *Chem. Soc. Rev.*, 2012, **41**, 7108–7146.
28 Z. Yang, *Adv. Biochem. Eng./Biotechnol.*, 2019, **168**, 31–59.
29 N. Guajardo, P. Domínguez de María, K. Ahumada, R. A. Schrebler, R. Ramírez-Tagle, F. A. Crespo and C. Carlesi, *ChemCatChem*, 2017, **9**, 1393–1396.
30 F. Gabriele, M. Chiarini, R. Germani, M. Tiecco and N. Spreti, *J. Mol. Liq.*, 2019, **291**, 111301.
31 T. El Achkar, S. Fourmentin and H. Greige-Gerges, *J. Mol. Liq.*, 2019, **288**, 111028.
32 N. Guajardo, K. Ahumada and P. Domínguez de María, *J. Biotechnol.*, 2020, **310**, 97–102.
33 N. Guajardo and P. Domínguez de María, *ChemCatChem*, 2019, **11**, 3128–3137.
34 O. S. Hammond, D. T. Bowron and K. J. Edler, *Angew. Chem., Int. Ed.*, 2017, **56**, 9782–9785.
35 P. Domínguez de María, N. Guajardo and S. Kara, in *Deep Eutectic Solvents: Synthesis, Properties, and Applications*, ed. D. J. Ramón and G. Guillena, Wiley-VCH Verlag GmbH, 2019, pp. 257–271.
36 L. Weng and M. Toner, *Phys. Chem. Chem. Phys.*, 2018, **20**, 22455–22462.
37 R. Wedberg, J. Abildskov and G. H. Peters, *J. Phys. Chem. B*, 2012, **116**, 2575–2585.
38 M. Shehata, A. Unlu, U. Sezerman and E. Timucin, *J. Phys. Chem. B*, 2020, **124**, 8801–8810.
39 P. Trodler and J. Pleiss, *BMC Struct. Biol.*, 2008, **8**, 9.
40 L. Huang, J. P. Bittner, P. Domínguez de María, S. Jakobtorweihen and S. Kara, *ChemBioChem*, 2020, **21**, 811–817.
41 P. Kumari, M. Kumari and H. K. Kashyap, *J. Phys. Chem. B*, 2020, **124**, 11919–11927.
42 S. L. Perkins, P. Painter and C. M. Colina, *J. Chem. Eng. Data*, 2014, **59**, 3652–3662.
43 S. L. Perkins, P. Painter and C. M. Colina, *J. Phys. Chem. B*, 2013, **117**, 10250–10260.
44 B. Doherty and O. Acevedo, *J. Phys. Chem. B*, 2018, **122**, 9982–9993.
45 A. González de Castilla, J. P. Bittner, S. Müller, S. Jakobtorweihen and I. Smirnova, *J. Chem. Eng. Data*, 2019, **65**, 943–967.
46 J. P. Bittner, L. Huang, N. Zhang, S. Kara and S. Jakobtorweihen, *J. Chem. Theory Comput.*, 2021, **17**, 5322–5341.
47 G. de Gonzalo, *Sustainable Chem.*, 2020, **1**, 290–297.
48 J. Wang, R. M. Wolf, J. W. Caldwell, P. A. Kollman and D. A. Case, *J. Comput. Chem.*, 2004, **25**, 1157–1174.
49 R. B. Best and G. Hummer, *J. Phys. Chem. B*, 2009, **113**, 9004–9015.
50 K. Vanommeslaeghe, E. Hatcher, C. Acharya, S. Kundu, S. Zhong, J. Shim, E. Darian, O. Guvench, P. Lopes, I. Vorobyov and A. D. Mackerell Jr., *J. Comput. Chem.*, 2010, **31**, 671–690.
51 W. Yu, X. He, K. Vanommeslaeghe and A. D. MacKerell Jr., *J. Comput. Chem.*, 2012, **33**, 2451–2468.
52 J. Huang, S. Rauscher, G. Nawrocki, T. Ran, M. Feig, B. L. de Groot, H. Grubmuller and A. D. MacKerell Jr., *Nat. Methods*, 2017, **14**, 71–73.
53 W. L. Jorgensen, D. S. Maxwell and J. Tirado-Rives, *J. Am. Chem. Soc.*, 1996, **118**, 11225–11236.
54 L. S. Dodda, I. Cabeza de Vaca, J. Tirado-Rives and W. L. Jorgensen, *Nucleic Acids Res.*, 2017, **45**, W331–W336.
55 D. A. Jahn, F. O. Akinkunmi and N. Giovambattista, *J. Phys. Chem. B*, 2014, **118**, 11284–11294.
56 C. Caleman, P. J. van Maaren, M. Hong, J. S. Hub, L. T. Costa and D. van der Spoel, *J. Chem. Theory Comput.*, 2012, **8**, 61–74.

57 M. J. Robertson, J. Tirado-Rives and W. L. Jorgensen, *J. Chem. Theory Comput.*, 2015, **11**, 3499–3509.
58 M. J. Robertson, Y. Qian, M. C. Robinson, J. Tirado-Rives and W. L. Jorgensen, *J. Chem. Theory Comput.*, 2019, **15**, 2734–2742.
59 W. L. Jorgensen, J. Chandrasekhar, J. D. Madura, R. W. Impey and M. L. Klein, *J. Chem. Phys.*, 1983, **79**, 926–935.
60 A. D. MacKerell, D. Bashford, M. Bellott, R. L. Dunbrack, J. D. Evanseck, M. J. Field, S. Fischer, J. Gao, H. Guo, S. Ha, D. Joseph-McCarthy, L. Kuchnir, K. Kuczera, F. T. Lau, C. Mattos, S. Michnick, T. Ngo, D. T. Nguyen, B. Prodhom, W. E. Reiher, B. Roux, M. Schlenkrich, J. C. Smith, R. Stote, J. Straub, M. Watanabe, J. Wiorkiewicz-Kuczera, D. Yin and M. Karplus, *J. Phys. Chem. B*, 1998, **102**, 3586–3616.
61 S. R. Durell, B. R. Brooks and A. Ben-Naim, *J. Phys. Chem.*, 2002, **98**, 2198–2202.
62 T. Darden, D. York and L. Pedersen, *J. Chem. Phys.*, 1993, **98**, 10089–10092.
63 M. J. Abraham, T. Murtola, R. Schulz, S. Páll, J. C. Smith, B. Hess and E. Lindahl, *SoftwareX*, 2015, **1–2**, 19–25.
64 M. J. Abraham, D. van der Spoel, E. Lindahl and B. Hess and T. G. D. Team, *GROMACS User Manual version 2019.4*, 2019.
65 H. Bekker, H. J. C. Berendsen, E. J. Dijkstra, S. Achterop, R. Vondrumen, D. Vanderspoel, A. Sijbers, H. Keegstra, B. Reitsma and M. K. R. Renardus, in *Physics Computing '92*, ed. R. A. DeGroot and J. Nadrchal, World Scientific Publishing, Singapore, 1993, pp. 252–256.
66 K. Kim and B. V. Plapp, *Biochemistry*, 2020, **59**, 862–879.
67 L. Martinez, R. Andrade, E. G. Birgin and J. M. Martinez, *J. Comput. Chem.*, 2009, **30**, 2157–2164.
68 S. Miyamoto and P. A. Kollman, *J. Comput. Chem.*, 1992, **13**, 952–962.
69 B. Hess, H. Bekker, H. J. C. Berendsen and J. G. E. M. Fraaije, *J. Comput. Chem.*, 1997, **18**, 1463–1472.
70 G. Bussi, D. Donadio and M. Parrinello, *J. Chem. Phys.*, 2007, **126**, 014101.
71 R. W. Hockney, *Methods Comput. Phys.*, 1970, 135–211.
72 H. J. C. Berendsen, J. P. M. Postma, W. F. van Gunsteren, A. DiNola and J. R. Haak, *J. Chem. Phys.*, 1984, **81**, 3684–3690.
73 M. Parrinello and A. Rahman, *J. Appl. Phys.*, 1981, **52**, 7182–7190.
74 A. Grossfield, P. N. Patrone, D. R. Roe, A. J. Schultz, D. W. Siderius and D. M. Zuckerman, *Living J. Comp. Mol. Sci.*, 2018, **1**, 5067.
75 R. Briones, C. Blau, C. Kutzner, B. L. de Groot and C. Aponte-Santamaria, *Biophys. J.*, 2019, **116**, 4–11.
76 C. Ma, A. Laaksonen, C. Liu, X. Lu and X. Ji, *Chem. Soc. Rev.*, 2018, **47**, 8685–8720.
77 G. Weiz, L. Braun, R. Lopez, P. Domínguez de María and J. D. Breccia, *J. Mol. Catal. B: Enzym.*, 2016, **130**, 70–73.
78 F. Chamouleau, C. Hagedorn, O. May and H. Gröger, *Flavour Fragrance J.*, 2007, **22**, 169–172.
79 C. Zhang, Q. Xu, H. Hou, J. Wu, Z. Zheng and J. Ouyang, *Microb. Cell Fact.*, 2020, **19**, 163.
80 P. J. Halling, *Biochim. Biophys. Acta*, 1990, **1040**, 225–228.
81 S.-H. Wu, A. R. Caparanga, R. B. Leron and M.-H. Li, *Thermochim. Acta*, 2012, **544**, 1–5.
82 E. Durand, J. Lecomte and P. Villeneuve, *Eur. J. Lipid Sci. Technol.*, 2013, **115**, 379–385.
83 F. Hollmann, I. W. C. E. Arends and D. Holtmann, *Green Chem.*, 2011, **13**, 2285–2314.
84 W. Humphrey, A. Dalke and K. Schulten, *J. Mol. Graphics*, 1996, **14**, 33–38.